Anisotropic magneto-Seebeck effect in the antiferromagnetic semimetal $FeGe_2$

Minori Hashizume,[1] Tomoyuki Yokouchi,[1,2,*] Kurea Nakagawa,[2] and Yuki Shiomi[1,2]
[1]*Department of Integrated Science, The University of Tokyo, Meguro, Tokyo 153-8902, Japan*
[2]*Department of Basic Science, The University of Tokyo, Meguro, Tokyo 153-8902, Japan*

(Received 8 April 2021; revised 26 June 2021; accepted 23 August 2021; published 7 September 2021)

We have investigated thermoelectric properties of the antiferromagnetic semimetal $FeGe_2$. As temperature decreases from 340 K, the Seebeck coefficient takes a maximum around the Néel temperature and then decreases to show a sign change from positive to negative <50 K. When a strong magnetic field is applied perpendicular to the sample plane, the sign change disappears, and the positive Seebeck coefficient is observed in the whole temperature range. This large magneto-Seebeck effect is anisotropic since the Seebeck coefficient is insensitive to in-plane magnetic fields. Based on the Mott formula, we discuss the origins for this anisotropic magneto-Seebeck effect.

DOI: 10.1103/PhysRevB.104.115109

I. INTRODUCTION

Thermoelectric conversion is one of the important key technologies for solving environmental issues since it enables the generation of electricity from waste heat without gas emission [1]. Extensive efforts have therefore been made to explore materials and physical mechanisms toward high-performance thermoelectric properties [2,3]. Investigating the magnetic field dependence of thermoelectric properties is an important issue since, although there is a possibility of the enhancement of thermoelectric properties by magnetic field, not many examples are reported, and its mechanism is not well understood. For example, it was recently found that the Seebeck coefficient in a chiral magnet is dramatically enhanced by an unconventional carrier scattering originating from critical spin fluctuations associated with a magnetic-field-induced topological phase transition of spin textures [4]. Furthermore, an anisotropic magneto-Seebeck effect can be used for a thermoelectric cooling and heating device [5]. Thus, it is important to explore materials that show a large anisotropic magneto-Seebeck effect and understand its mechanism.

To further deepen the understanding of magnetothermoelectric phenomena, we here focus on $FeGe_2$. The crystal structure of $FeGe_2$ belongs to the space group $I4/mcm$ [inset to Fig. 1(a)] [6–9]. $FeGe_2$ exhibits two magnetic phase transitions: a paramagnetic-to-incommensurate spin-density wave (SDW) transition at $T_{N1} \sim 289$ K and incommensurate-to-commensurate SDW transition at $T_{N2} \sim 264$ K [10]. In the SDW states, magnetic moments lie on the ab plane [9,11–13]. The system shows a good metallic conduction with the residual resistance ratio >50 [11]. A large magnetoresistance (MR) >1000% is observed at low temperatures [11]. This large MR is only observed when the magnetic field is applied perpendicular to the electric current regardless of its direction against the crystal structure, suggesting that this is caused not by magnetic origins but by the Lorentz force acting on high-mobility carriers. Consistent with the high-mobility transport at low temperatures, Shubnikov–de Haas oscillations have also been observed in magnetic fields stronger than 8.4 T at 0.3 K [11]. According to a band calculation [14], $FeGe_2$ can be classified as a semimetal due to the overlap of the Fe 3d and Ge 4p bands at the Fermi level. The flat Fe 3d band pocket constitutes a high peak in the total density of states (DOS) near the Fermi level. This large change in DOS near the Fermi level is promising for an efficient thermoelectric conversion. Additionally, the presence of high-mobility carriers at low temperatures [11] seems to contradict heavy mass presumed for Fe 3d carriers with the flat band, and thus, the Seebeck effect sensitive to carrier types should be a useful probe to elucidate the transport properties of $FeGe_2$.

In this paper, we investigate the Seebeck effect in $FeGe_2$ single crystals with and without external magnetic fields. Under zero magnetic field, the Seebeck coefficient of positive sign shows a maximum at around the antiferromagnetic transition temperatures. With decreasing temperature, the sign of the Seebeck coefficient changes from positive to negative, showing two-carrier transport in $FeGe_2$. The power factor reaches 60 μW cm^{-1}K^{-2} at low temperatures (see Appendix). When the magnetic field is applied perpendicular to the temperature-gradient direction, the negative Seebeck coefficient is suppressed, and the sign changes from negative to positive under strong magnetic fields. Such a pronounced magneto-Seebeck effect is not observed when the magnetic field is applied parallel to the temperature-gradient direction. We discuss the anisotropic magneto-Seebeck effect based on the Mott formula.

II. EXPERIMENT

Single crystals of $FeGe_2$ were prepared by a slow-cooling method from high-purity iron and germanium powders. The powders were mixed and heated in an evacuated quartz tube at 800 ° in 15 h. After keeping the temperature for 4 d, the

*yokouchi@g.ecc.u-tokyo.ac.jp

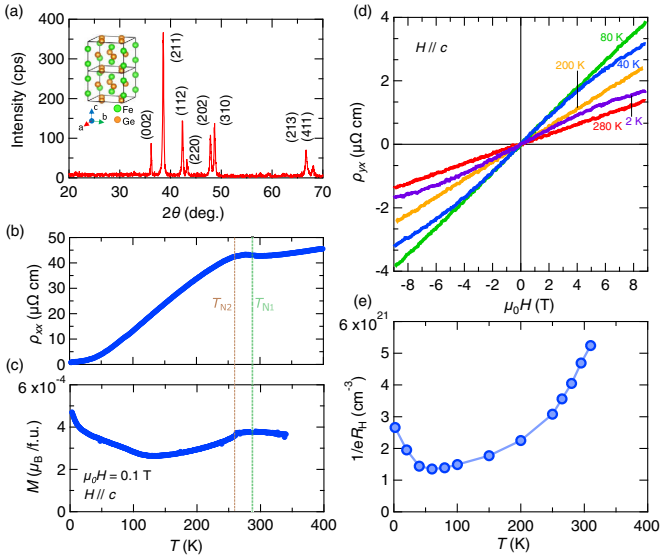

FIG. 1. (a) Powder x-ray diffraction pattern and Miller indices of $FeGe_2$. The crystal structure of $FeGe_2$ is shown in the inset. (b) Temperature dependence of resistivity. The two transition temperatures (T_{N1} and T_{N2}) are denoted by the dotted lines. (c) Temperature dependence of magnetization measured in the magnetic field of 0.1 T applied parallel to the c axis. (d) Magnetic field dependence of the Hall resistivity at selected temperatures. (e) Temperature dependence of the inverse of the Hall coefficient $1/(R_{\rm H}e)$. Below 60 K, the data of -3 to 3 T are used to determine $R_{\rm H}e$ (see text).

temperature was raised to 900 ° in 5 h and kept for 1 d. Then the temperature was cooled to 800 ° in 50 h and kept for 1 d, followed by cooling down to room temperature in 12 h. The single-phase $FeGe_2$ was obtained, as confirmed by powder x-ray diffraction in Fig. 1(a).

The obtained ingots were easily cleaved in the *ab* plane. For measurements of magnetization and transport properties, two platelike samples (sample1 and sample2) with the *ab* plane as the largest surface were prepared. Here, these two samples were prepared by dividing a plate-shaped sample into two. Hence, the difference in qualities and physical properties between sample1 and 2 was expected to be minimum. The sample sizes were 3.5–4.0 mm (length) × 1.75 mm (width) × 0.41 mm (thickness) and 3.5–4.0 mm (length) × 1.0 mm (width) × 0.41 mm (thickness). The longitudinal resistivity and Hall resistivity were measured using the Physical Property Measurement System (PPMS; Quantum Design). The Seebeck coefficient and thermal conductivity were measured by a steady state method using a homemade sample holder in PPMS [15]. In all the transport measurements, electric and heat currents were applied within the *ab* plane. The magnetization of the sample was measured using the Magnetic Property Measurement System (Quantum Design) by applying 0.1 T of magnetic field perpendicular to the *ab* plane.

III. RESULTS AND DISCUSSION

First, temperature dependence of resistivity ρ_{xx} is shown in Fig. 1(b). The resistivity is metallic with the residual resistance ratio of 58 and shows a hump structure around room temperature. This hump structure is attributed to the SDW transition. The two transition temperatures are defined from the temperature derivative of the measured resistivity; the first transition temperature T_{N1} (paramagnet-to-incommensurate SDW transition) is the temperature at which the differential of the resistivity is minimum, and the second transition temperature T_{N2} (incommensurate-to-commensurate SDW transition) is where the differential of the resistivity changes discontinuously. The transition temperatures in our sample ($T_{N1} = 284$ K and $T_{N2} = 264$ K) are in fair agreement with previous research ($T_{N1} \sim 289$ K and $T_{N2} \sim 264$ K) [11]. The resistivity takes a maximum just below T_{N1}. Similar behavior is also observed at the paramagnetic-to-SDW transition temperature in Cr [16], resulting from the formation of an energy gap near the Fermi level due to the SDW transition [17,18]. The temperature dependence of the magnetization is shown in Fig. 1(c). The apparent change of the magnetization at T_{N2} can be seen, consistent with the previous report [19].

The magnetic field dependence of Hall resistivity at various temperatures is shown in Fig. 1(d). Here, magnetic field (H) was applied perpendicular to the *ab* plane. The slope of the Hall resistivity is positive in the entire temperature range. This suggests that the dominant carriers of $FeGe_2$ are holes. Above 80 K, the Hall resistivity is H linear in the whole field range, while that <60 K is clearly nonlinear >3 T. The nonlinearity of the Hall resistivity indicates the presence of multiple carriers, as suggested from the band calculation [14]. In the case of two carriers, the Hall resistivity is expressed with four parameters [20]: carrier mobilities (μ_h and μ_e) and carrier densities (n_h and n_e). The subscripts h and e refer to holes and electrons, respectively. At low temperatures, electrons also contribute to the transport properties, as can be confirmed from the nonlinearity of the Hall resistivity.

We assume that the Hall resistivity is linear with the magnetic field in the low-field regime from -3 to 3 T, and the Hall coefficient is estimated by $R_{\rm H} = \rho_{yx}/B$. At each temperature, $1/(R_{\rm H}e)$ is plotted in Fig. 1(e). The magnitude at 300 K is $\sim 5 \times 10^{21}$ cm^{-3}. This magnitude of carrier density is lower than conventional metals ($\sim 10^{23}$ cm^{-3}), consistent with semimetallic transport in $FeGe_2$. With decreasing temperature, $1/(R_{\rm H}e)$ decreases and then starts to increase < 40 K.

The temperature dependence of the Seebeck coefficient measured under zero magnetic field is shown in Fig. 2. The Seebeck coefficient S is defined with the following equation: $E = S\nabla T$, where E is the generated electric field and ∇T the temperature gradient. In the single-carrier model, the following relation stands according to the type of carriers: $S > 0$ for hole carriers and $S < 0$ for electrons. The observed sign of S is positive at room temperature, consistent with the dominant hole conduction observed in the Hall effect. As temperature decreases from 340 K, S takes a maximum at 250 K, just below T_{N2}. A similar peak is observed in a typical SDW system Cr as well and attributed to the formation of an energy gap upon the SDW transition [21]. We note the Seebeck coefficient does not show a large change at the paramagnetic-to-incommensurate transition temperature T_{N1}. This is probably because the incommensurate SDW has little effect on the band structure in the case of $FeGe_2$. With further decreasing temperature, S decreases and notably shows a sign change from positive to negative at 50 K. The Seebeck

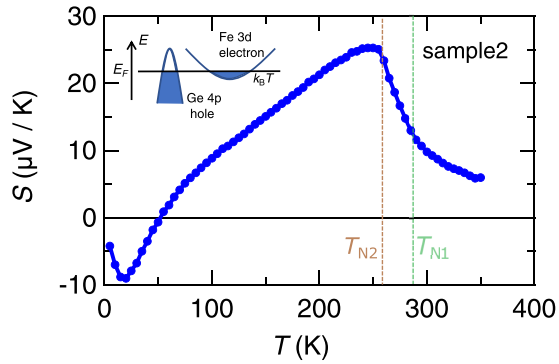

FIG. 2. Temperature dependence of the Seebeck coefficient under zero magnetic field. The paramagnetic-to-incommensurate spin-density wave (SDW) transition temperature (T_{N1}) and the incommensurate-to-commensurate SDW transition temperature (T_{N2}) determined by the resistivity measurement are shown with the dotted lines. A simplified band structure near the Fermi level is schematically illustrated in the inset.

effect at low temperatures is dominated not by holes but by electrons.

As mentioned in the introduction, the band structure of $FeGe_2$ was calculated in previous research, in which the Ge $4p$ band lies from -6 eV to the Fermi energy (E_F), and the flat Fe $3d$ band is dominant near E_F [14]. Hence, we adopt the following two-band model: holes with small effective mass, thus leading to high mobility, are provided by the Ge $4p$ band with wide band width, and electrons with large effective mass, thus low mobility, are provided by the shallow Fe $3d$ band with narrow band width, as illustrated in the inset to Fig. 2. This simple model explains well the observed temperature dependences of both the Hall resistivity and the Seebeck effect. Since the Hall resistivity depends on carrier densities and mobilities for holes and electrons [20], the holes with high mobility mainly contribute to the Hall effect over the whole temperature range. The electrons with heavy mass are not important in the Hall transport. As for the Seebeck effect, in contrast, since the flat Fe $3d$ band is shallow and a large change in DOS is expected in the energy range between $E_F \pm k_B T$, where k_B is the Boltzmann constant, Fe $3d$ electrons with low mobility can also contribute to the Seebeck effect through the Mott formula [Eqs. (1) and (3)]. At high temperatures, holes of the Ge $4p$ band are dominant in the Seebeck effect, while at sufficiently low temperatures where the Seebeck coefficient from Ge $4p$ holes is reduced, electrons in the narrow, shallow Fe $3d$ electron band gain a larger influence on the Seebeck effect, and thus, the Seebeck coefficient becomes negative.

Next, we have measured the Seebeck coefficient under magnetic fields. The temperature dependence of the Seebeck coefficient under the magnetic field applied perpendicular to the *ab* plane is shown in Fig. 3(a). Above T_{N2}, the Seebeck coefficient is almost independent of the magnetic field. In contrast, below T_{N2}, the Seebeck coefficient becomes larger with increasing magnetic field, and the change is especially pronounced at low temperatures. Notably, while the Seebeck coefficient at 0 T turned negative at low temperatures, the Seebeck coefficient at 9 T is positive for the whole temperature range. We also measured the isothermal magnetic field dependence of the Seebeck coefficient [Fig. 3(b)]. Again, the Seebeck coefficient increases and becomes positive with magnetic field at low temperatures. On the contrary, the change in the Seebeck coefficient with the magnetic field is small and the field-induced sign change is not observed when the magnetic field is applied parallel to the temperature-gradient direction [Figs. 3(c) and 3(d)]. We note that a difference in the value of the Seebeck coefficient at zero magnetic field between $H \perp \Delta T$ and $H // \Delta T$ is simply due to uncertainty in measuring the electrode distance. In addition, the Seebeck coefficients for *S*-*T* curves at zero magnetic field are in good agreement with those for *S*-*H* curves, indicating the reliability of the measurement.

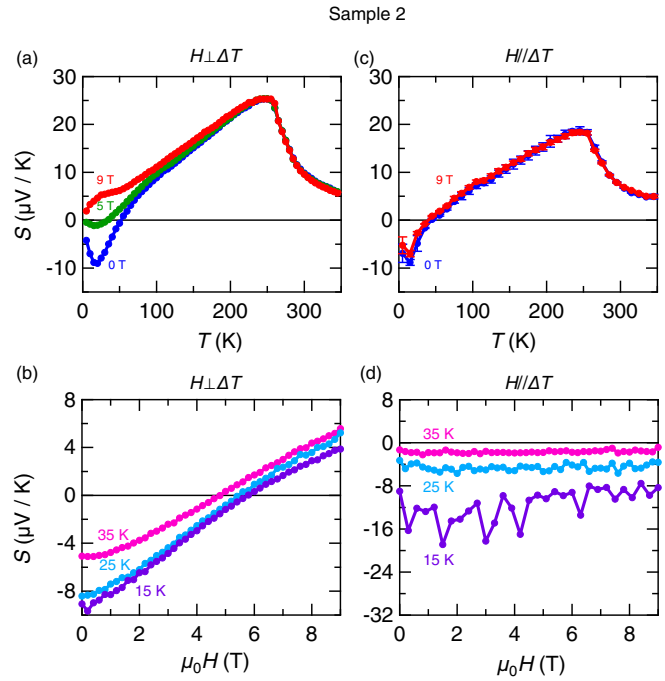

FIG.3. Temperature dependence of the Seebeck coefficient under selected magnetic fields applied (a) perpendicular to the *ab* plane ($H \perp \nabla T$) and (c) parallel to the temperature gradient ($H // \nabla T$). Magnetic field dependence of the Seebeck coefficient at low temperatures (b) for $H \perp \nabla T$ and (d) for $H // \nabla T$. Error bars correspond to the standard deviation of two measurements.

To analyze the magnetic field dependence of the Seebeck coefficient, we bring out the Mott formula. The Mott formula describes the Seebeck coefficient and is given by [20,22]

$$S = \frac{\pi^2 k_B^2 T}{3e}\left(\frac{\sigma^2}{\sigma^2 + \sigma_{xy}^2}\frac{\partial \ln\sigma}{\partial E}\bigg|_{E=E_F} + \frac{\sigma_{xy}^2}{\sigma^2 + \sigma_{xy}^2}\frac{\partial \ln\sigma_{xy}}{\partial E}\bigg|_{E=E_F}\right). \quad (1)$$

Here, k_B, σ, and σ_{xy} are the Boltzmann constant, electrical conductivity, and Hall conductivity, respectively. The contribution from the transverse responses [the second term in Eq. (1)] is one possible origin of the magneto-Seebeck effect. When σ_{xy} and $\frac{\partial \ln\sigma_{xy}}{\partial E}$ are not small compared with the

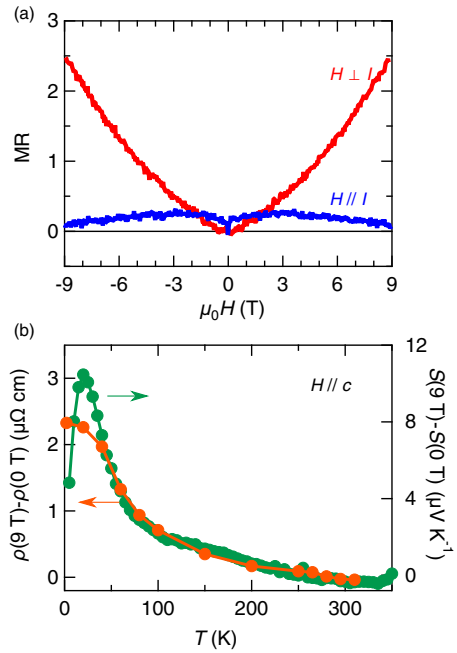

FIG. 4. (a) Magnetic field dependence of resistivity [magnetoresistance (MR)] at 2 K for the magnetic field perpendicular to the *ab* plane ($H\perp I$) and parallel to the current ($H//I$). For the definition of MR, see text. (b)Temperature dependences of $\Delta S = S(9\,\mathrm{T}) - S(0\,\mathrm{T})$ and $\Delta\rho = \rho(9\,\mathrm{T}) - \rho(0\,\mathrm{T})$ measured with $H//c$ axis ($H\perp I$, $H\perp\nabla T$).

longitudinal responses (σ and $\frac{\partial \ln\sigma}{\partial E}$), the second term in Eq. (1) also contributes to the Seebeck coefficient. In this case, the observed anisotropic magneto-Seebeck effect and magnetic-field-induced sign reversal can be explained by Eq. (1), if the signs of $\frac{\partial \ln\sigma}{\partial E}$ and $\frac{\partial \ln\sigma_{xy}}{\partial E}$ are negative and positive, respectively; at zero magnetic field, since σ_{xy}^2 is zero, the first term originates the negative S. With increasing the magnetic field parallel to the c axis, the second term becomes dominant over the first term, leading to positive S.

Other possible origins of the observed magnetic field profile of the Seebeck effect are the magnetic field dependence of the DOS and the magnetic field dependence of the energy derivative of the mobility. When there are both holes and electrons as transport carriers [23], the overall Seebeck coefficient is described as

$$S = \frac{\sigma_h S_h + \sigma_e S_e}{\sigma_h + \sigma_e} = \frac{\sigma_h}{\sigma_h + \sigma_e}\left(\frac{\pi^2 k_B^2 T}{3e}\frac{\sigma_h'}{\sigma_h}\right) + \frac{\sigma_e}{\sigma_h + \sigma_e}\left(\frac{\pi^2 k_B^2 T}{3e}\frac{\sigma_e'}{\sigma_e}\right) = \frac{\pi^2 k_B^2 T}{3e}\frac{\sigma_h' + \sigma_e'}{\sigma_h + \sigma_e}, \quad (2)$$

where $\sigma_h = n_e e\mu_e$, $\sigma_h = n_h e\mu_h$. Here, we ignore the transverse responses (i.e., σ_{xy} and $\frac{\partial \ln\sigma_{xy}}{\partial E}$). This suggests that the Seebeck coefficient is proportional to resistivity $1/(\sigma_h + \sigma_e)$ if the energy derivative of conductivity is constant.

To discuss the magneto-Seebeck effect based on Eq. (2), we first examine the MR measured with the magnetic field applied perpendicular to the *ab* plane and parallel to the current direction. The MR $= [\rho(B) - \rho(0\,\mathrm{T})]/\rho(0\,\mathrm{T})$ measured in the two magnetic field conditions at 2 K is shown in Fig. 4(a). When the magnetic field is applied perpendicular to the plane, the MR increases with increasing the magnetic field, and the positive MR reaches 250% at 9 T. In contrast, when the magnetic field is applied parallel to the current direction, the MR is ∼0 at 9 T. These results are consistent with the previous report [11].

In Fig. 4(b), we compare $\Delta S = S(9\,\mathrm{T}) - S(0\,\mathrm{T})$ and $\Delta\rho = \rho(9\,\mathrm{T}) - \rho(0\,\mathrm{T})$ for the magnetic field applied perpendicular to the *ab* plane. Above 70 K, ΔS and $\Delta\rho$ are found to be almost proportional to each other. From Eq. (2), if $\sigma'(=\sigma_h' + \sigma_e')$ is constant with the magnetic field, i.e., $\sigma'(9\,\mathrm{T}) = \sigma'(0\,\mathrm{T})$, ΔS can scale with $\Delta\rho$. In contrast, <70 K, temperature dependence of ΔS deviates from that of $\Delta\rho$; as seen from Fig. 4(b), $\Delta S/\Delta\rho < 70$ K is larger than that >70 K. This suggests $\sigma'(9\,\mathrm{T}) > \sigma'(0\,\mathrm{T}) < 70$ K. In other words, the σ' term plays an important role in the magnetic field dependence of S at low temperatures. In the semiclassical transport theory, σ' can be decomposed to

$$\sigma' = \sigma_h' + \sigma_e' = \frac{\partial}{\partial E}(\sigma_h + \sigma_e)|_{E_F} = \frac{\partial}{\partial E}(n_h e\mu_h + n_e e\mu_e)|_{E_F} = \frac{\partial n_h}{\partial E}|_{E_F} e\mu_h + n_h e\frac{\partial \mu_h}{\partial E}|_{E_F} + \frac{\partial n_e}{\partial E}|_{E_F} e\mu_e + n_e e\frac{\partial \mu_e}{\partial E}|_{E_F}. \quad (3)$$

Hence, the magnetic field dependence of σ' results from the magnetic field dependence of the DOS $D_{h/e} = \frac{\partial n_{h/e}}{\partial E}|_{E_F}$ and/or the energy derivative of the mobility $\frac{\partial \mu_{h/e}}{\partial E}|_{E_F}$. The magnetic field dependence of $\frac{\partial \mu_{h/e}}{\partial E}|_{E_F}$ is caused by the magnetic field dependence of the energy derivative of scattering rate τ, which was previously observed in MnGe [4].

IV. SUMMARY

In conclusion, we investigated the temperature and magnetic field dependence of the Seebeck effect as well as other

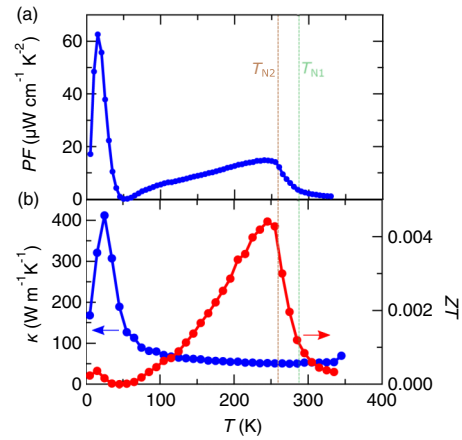

FIG. 5. (a) Temperature dependence of the power factor (PF) under zero field. For the definition of PF, see text. (b) Temperature dependence of thermal conductivity (blue) and the figure of merit (ZT; red). The paramagnetic-to-incommensurate spin-density wave (SDW) transition temperature (T_{N1}) and the incommensurate-to-commensurate SDW transition temperature (T_{N2}) determined by the resistivity measurement are shown with the dotted lines.

transport effects for $FeGe_2$ single crystals. The sign of the Seebeck coefficient is positive >50 K, while it is negative <50 K under zero magnetic field. The sign change in the Seebeck coefficient at 50 K is explained by competition between the positive Seebeck coefficient from a Ge $4p$ light hole band and the negative one from a Fe $3d$ heavy electron band with a large DOS change near the Fermi level. The effect of electron transport at low temperatures is also observed in the Hall effect. Furthermore, when the magnetic field is applied perpendicular to the temperature gradient, the low-temperature Seebeck coefficient significantly depends on the magnetic field, and the sign change is suppressed down to the lowest temperature. Based on the Mott formula, we have discussed the three possible origins for the observed magneto-Seebeck effect: the contribution of the transverse response, the magnetic field dependence of the DOS, and the magnetic field dependence of the energy derivative of the scattering rate τ.

ACKNOWLEDGMENTS

This paper was supported by Japan Society for the Promotion of Science KAKENHI under Grants No. JP21H01794, No. JP20H05153, No. JP20H04631, No. JP19K22124, No. JP19H05600, No. JP19H02424, and No. JP19K14667.

APPENDIX

The power factor (PF) is one of the factors to evaluate the performance of a thermoelectric device. The PF is proportional to the electric power generated per unit temperature gradient and given by $\mathrm{PF} = S^2/\rho_{xx}$. The PF calculated from the resistivity and Seebeck coefficient measured under zero magnetic field is shown as a function of temperature in Fig. 5(a). The PF exhibits two peaks and notably exceeds 60 $\mu\mathrm{W\,cm^{-1}K^{-2}}$ at the lower peak. The very low resistivity due to high-mobility holes and the Seebeck coefficient due to electrons give rise to the relatively large PF at low temperatures. The thermal conductivity κ for this material under zero field is shown in blue in Fig. 5(b). Using κ as well as S and ρ_{xx}, we calculate the figure of merit $\mathrm{ZT} = S^2T/\kappa\rho_{xx}$ and plot ZT as a function of temperature in Fig. 5(b) (red color). Like the PF, the ZT shows two peaks. The peak amplitude at 250 K is 0.0045 and larger than that of the low-temperature peak owing to the higher temperature and smaller κ.

[1] G. D. Mahan, Solid State Phys. **51**, 81 (1998).
[2] X.-L. Shi, J. Zou, and Z.-G. Chen, Chem. Rev. **120**, 7399 (2020).
[3] J. Mao, Z. Liu, J. Zhou, H. Zhu, Q. Zhang, G. Chen, and Z. Ren, Adv. Phys. **67**, 69 (2018).
[4] Y. Fujishiro, N. Kanazawa, T. Shimojima, A. Nakamura, K. Ishizaka, T. Koretsune, R. Arita, A. Miyake, H. Mitamura, K. Akiba, M. Tokunaga, J. Shiogai, S. Kimura, S. Awaji, A. Tsukazaki, A. Kikkawa, Y. Taguchi, and Y. Tokura, Nat. Commun. **9**, 408 (2018).
[5] K. I. Uchida, S. Daimon, R. Iguchi, and E. Saitoh, Nature (London) **558**, 95 (2018).
[6] K. Yasukōchi, K. Kanematsu, and T. Ohoyama, J. Phys. Soc. Japan **16**, 429 (1961).
[7] E. Krén and P. Szabó, Phys. Lett. **11**, 215 (1964).
[8] J. Sólyom and E. Krén, Solid State Commun. **4**, 255 (1966).
[9] L. M. Corliss, J. M. Hastings, W. Kunnmann, R. Thomas, J. Zhuang, R. Butera, and D. Mukamel, Phys. Rev. B **31**, 4337 (1985).
[10] T. E. Mason, C. P. Adams, S. A. M. Mentink, E. Fawcett, A. Z. Menshikov, C. D. Frost, J. B. Forsyth, T. G. Perring, and T. M. Holden, Physica B **237**, 449 (1997).
[11] C. P. Adams, T. E. Mason, S. A. M. Mentink, and E. Fawcett, J. Phys. Condens. Matter **9**, 1347 (1997).
[12] J. B. Forsyth, C. E. Johnson, and P. J. Brown, Philos. Mag. **10**, 713 (1964).
[13] V. V. Tarasenko, V. Pluzhnikov, and E. Fawcett, Phys. Rev. B **40**, 471 (1989).
[14] T. Jeong, Solid State Commun. **141**, 329 (2007).
[15] K. Nakagawa, H. Asano, Y. Miyazaki, and Y. Shiomi, J. Appl. Phys. **126**, 183904 (2019).
[16] E. Fawcett, Rev. Mod. Phys. **60**, 209 (1988).
[17] G. Grüner, *Density Waves in Solids* (Perseus publishing, Cambridge, MA, 1994).
[18] L. L. Van Zandt and A. W. Overhauser, Phys. Rev. **141**, 583 (1966).
[19] P. D. Babu, P. K. Mishra, V. Dube, R. Mishra, P. U. Sastry, and G. Ravikumar, AIP Conf. Proc. **1591**, 1586 (2014).
[20] J. M. Ziman, *Electrons and Phonons: The Theory of Transport Phenomena in Solids* (Oxford University Press, Oxford, 2001).
[21] E. Fawcett, H. L. Alberts, V. Y. Galkin, D. R. Noakes, and J. V. Yakhmi, Rev. Mod. Phys. **66**, 25 (1994).
[22] T. Liang, Q. Gibson, J. Xiong, M. Hirschberger, S. P. Koduvayur, R. J. Cava, and N. P. Ong, Nat. Commun. **4**, 2696 (2013).
[23] K. Wang, D. Graf, and C. Petrovic, Phys. Rev. B. **89**, 125202 (2014).